HiSST: 3rd International Conference on
High-Speed Vehicle Science Technology
14 -19 April 2024, Busan, Korea

A Numerical Simulation on the Unsteady Flow in a GCH_4-GOx Small Thrust Chamber

Hong Yeong Park[1], Yun Hyeong Kang[2], Chang Han Bae[3], Jeong Soo Kim[4]

Abstract

A numerical simulation was conducted to scrutinize an unsteady physics which shows a stepwise increase of thrust performance in the later part of the combustion under the fuel-rich conditions. The nozzle outflow region was included in the calculation domain to reflect the influence of the atmospheric pressure condition. The flow field was analyzed using the RANS (Reynolds-Averaged Navier-Stokes) equation, and a non-adiabatic diffusion flamelet with 21 species and 84 reactions was applied to simulate the flame structure. As a result, the pressure and thrust calculated by the simulations were in good agreement with the experimental ones. However, an abrupt increase of thrust performance observed at the later stage of the combustion duration was not clearly captured in the transient results. This indicates a limitation of the combustion model employed in calculating the abnormal phenomenon of thrust change.

Keywords: *CFD (Computational Fluid Dynamics), Methane, Non-premixed combustion*

Nomenclature

Latin
k – Turbulent kinetic energy
G_k – Generation term
M_t – Turbulent Mach number
S – Modulus of mean rate of strain tensor
u_i – Velocity
Y_i – Mass fraction of i-th species
Z – Mixture fraction
C^*– Characteristic velocity
C_P – Specific heat
h – Enthalpy
t – Time
T – Temperature
$\dot{m}_t$ – Total mass flow rate
Greek
χ – Scalar dissipation rate
ε – Turbulent dissipation rate
$\sigma_k, \sigma_\varepsilon$ – Constants in turbulence transport equation
μ – Dynamic viscosity
ν – Kinematic viscosity
μ_t – Turbulent viscosity
$\dot{\omega}_i$ – Mass production rate of i-th species
ρ – Density
ϕ – Equivalence ratio

1. Introduction

The combustion efficiency and ignition stability based on propellant supply conditions are the valuable information to develop the optimized rocket engine. However, achieving optimal conditions in liquid rocket engines requires testing under various operating conditions and this can be time-consuming, costly, and also risky. To reduce these development costs in a constrained environment, numerical

[1] *Pukyong National University, 48513 Busan, Republic of Korea, hypark@pukyong.ac.kr*
[2] *Pukyong National University, 48513 Busan, Republic of Korea, yhkang@pukyong.ac.kr*
[3] *Pukyong National University, 48513 Busan, Republic of Korea, chbae@pukyong.ac.kr*
[4] *Pukyong National University, 48513 Busan, Republic of Korea, jeongkim@pknu.ac.kr*

investigations can be employed. Numerical analyses have the advantage of extracting crucial design factors in advance when experimental data is limited. In addition, validated calculation methods can provide information on the internal flow characteristics of the combustion chamber that are hard to obtain through experimental tests.

Several numerical studies have been conducted to analyze the mixing and combustion process of propellants as part of the development of liquid rocket engines. Cheng and Farmer [1] developed the CFD spray combustion model to understand flow physics of the injector under various engine-operating conditions. Liang et al. [2] presented an analytical model for simulating three-phase transient combustion flows in a thrust chamber and calculated the interactions between the phases. Urbono et al. [3] analyzed the combustion instability of the liquid rocket engine using the LES (Large Eddy Simulation), and found that the oscillatory regime and flame structure were similar to the features observed from the experiment.

In this paper, prior to establishing a way to predict the performances of a small rocket engine employing methane and liquid oxygen as propellant, a numerical simulation was performed to calculate combustion behavior in a small GCH_4-GOx combustion chamber. All the analyses were simulated in a transient state to observe the variations in thrust performances over time and the constructed calculation model was verified by comparing with the experimental data obtained from the in-house hot-firing test [4].

2. Numerical method

2.1. Turbulence model

An analysis on the flow field in the thrust chamber involves the mixing and combustion processes of the propellants. Therefore, an appropriate selection of the turbulence model is required. For the calculation of the turbulent flow, the compressible realizable k-ε model [5] was used. The flow through the converging-diverging nozzle reaches a supersonic state, and interactions of various physical phenomena occur within this flow field. To predict the characteristics of the high-speed compressible flow, Sakar et al. [6] developed a compressible dissipation term in the turbulent kinetic energy equation, as shown in Eq. 1. Here, the model constant was set as $\alpha_1 = 1$.

$$\varepsilon_c = \alpha_1 \varepsilon M_t^2 \tag{1}$$

Realizable k-ε model computes the two differential equations with the turbulent kinetic energy and the turbulent dissipation rate as the dependant variables, and these model with compressibility correction are defined by Eq. 2 and Eq. 3 respectively. The compressible dissipation term added in the equation of turbulent kinetic energy accounts for the turbulent energy reduction with increasing Mach numbers so that enhances the predictive performance of turbulent flow [7].

$$\rho \frac{\partial k}{\partial t} + \frac{\partial (\rho k u_i)}{\partial x_i} = \frac{\partial}{\partial x_i}\left[\left(\mu + \frac{\mu_t}{\sigma_k}\right)\frac{\partial k}{\partial x_i}\right] + G_k - \rho\varepsilon(1 + M_t^2) \tag{2}$$

$$\rho \frac{\partial \varepsilon}{\partial t} + \frac{\partial (\rho \varepsilon u_i)}{\partial x_i} = \frac{\partial}{\partial x_i}\left[\left(\mu + \frac{\mu_t}{\sigma_\varepsilon}\right)\frac{\partial \varepsilon}{\partial x_i}\right] + \rho\varepsilon C_{1\varepsilon} S - C_{2\varepsilon}\rho \frac{\varepsilon^2}{k + \sqrt{\nu\varepsilon}} \tag{3}$$

2.2. Combustion model

The non-adiabatic diffusion flamelet model was utilized to simulate non-premixed combustion [8]. The diffusion flamelet model is the analytical method assuming the turbulent flame field as a set of laminar flamelets in one-dimension with the micro-structure of the flame being governed by the scalar dissipation rate [9]. The differential equations in one-dimensional form for non-adiabatic flamelet are derived under the assumption of the unity Lewis number for all species, being described as Eq. 4 and Eq. 5 below [10]. In this study, a steady diffusion flamelet model was used based on 21 chemical species and 84 reactions from DRM-19 mechanism [11], and the database on the flamelet was calculated using the inlet temperature of $298\ \mathrm{K}$ and the operating pressure from the practical test case.

$$\frac{\partial Y_i}{\partial t} = \frac{\chi}{2}\frac{\partial^2 Y_i}{\partial Z^2} + \frac{\dot{\omega}_i}{\rho} \tag{4}$$

$$\frac{\partial T}{\partial t} = \frac{\chi}{2}\frac{1}{C_P}\frac{\partial^2 h}{\partial Z^2} - \frac{1}{\rho C_P}\sum_{i=1}^{N} h_i\,\dot{\omega}_i \tag{5}$$

3. Test Description

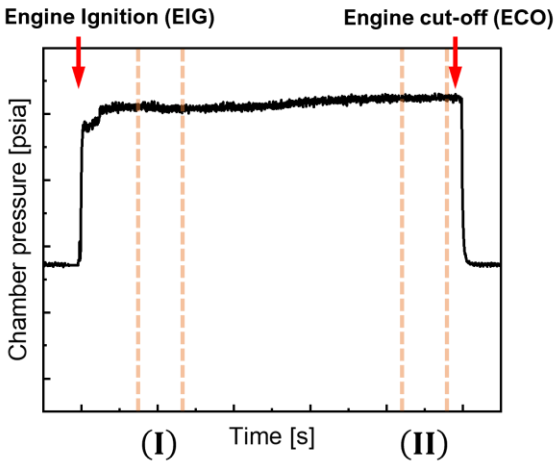

Fig. 1. Two sections whose data was reduced over the combustion period.

Table 1. Experimental cases employed in the current calculations.

Equivalence ratio, ϕ	Relative rise of C^* [%]	Cases identifier	Combustion time
2.00	0.06	GE1	$10\ s$
3.65	2.17	GE6	$15\ s$
5.36	6.28	GE11	$20\ s$

As a part of the preliminary study to predict combustion behavior of liquid rocket combustor using bi-propellants, an analysis was performed on the GCH_4-GOx thrust chamber and the analytical model was constructed based on the experimental measurements obtained from the in-house hot-firing test. The test aimed to verify the combustion performance of the GCH_4-GOx combustor under the very fuel-rich conditions. The mass flow rate of GOx was fixed at $12\ \mathrm{g/s}$ so that the equivalence ratios could be determined by the mass flow rate of GCH_4 only. As a result, a distinct rise of the characteristic velocity was observed at the later stage of the firing duration. The greater the equivalence ratio was, the more severe the distinct rise was.

To compare the variations over the period by cases, two periods within the combustion duration were selected as shown in Fig. 1. Period (I) was set from $3.01\ \mathrm{s}$ to $5.5\ \mathrm{s}$ after the engine ignition (EIG, Engine Ignition), and period (II) was set during the $3\ \mathrm{s}$ before the propellant supply valve closure (ECO, Engine Cut-off). Table 1 lists up the test cases to be simulated and their respective performance variation within the firing time according to the equivalence ratio. All the cases were tried to simulate in a transient state and the variations in pressure and characteristic velocity over the entire combustion time were observed.

4. Numerical setup

Table 2 represents the boundary conditions used in this calculation. At the inlet, the temperature values for both methane and oxygen were assumed to be $298\ \mathrm{K}$ and the mass flow rates of propellants

measured from the experiment were used. Since the measurement of the wall temperature in the experiment was made only up to the lower part of the chamber, those of the nozzle part were supplemented with the aid of NASA CEA (Chemical Equilibrium with Application) code [12] to set the overall temperature profile for wall boundary condition. The injector face, excluding the propellant injection region, was assigned adiabatic and no-slip condition.

Table 2. Boundary conditions used in the current calculation.

Boundary	Momentum	Energy
Inlet of GCH_4/GOx	Mass flow rate	298 K
Injector face	No-slip wall	Adiabatic
Chamber wall	No-slip wall	Temperature profile
Axis	Axisymmetric	

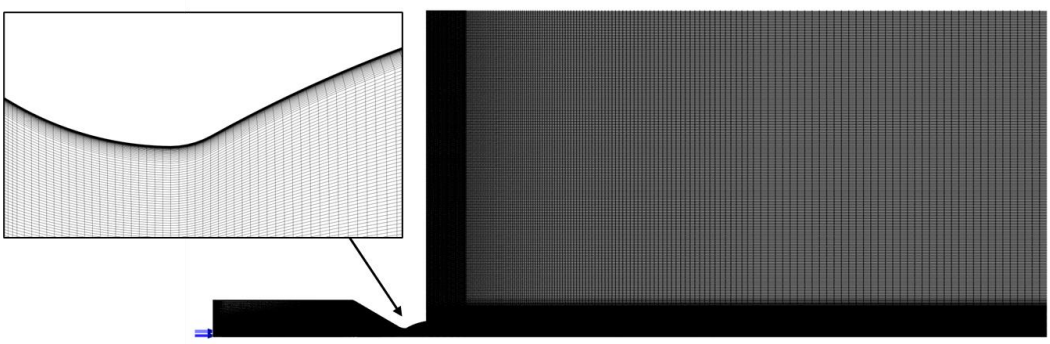

Fig. 2. Grid system in the full computational domain.

Fig. 2 displays the full grid domain used for the numerical calculation, with an enlarged view of the nozzle throat. The computational domain includes the outflow field of supersonic nozzle to reflect the influence by the outlet of atmospheric condition, and it was set to be 10 times larger radially and 20 times larger axially than the diameter of nozzle exit. The grid system consists of 154,600 quadrilateral cells and 155,666 nodes. The first cell thickness in radial direction from the chamber wall was set to 9.4×10^{-5} mm to improve the accuracy of the boundary layer calculation. The internal flow field of the thrust chamber was analyzed with the RANS (Reynolds-Averaged Navier Stokes) equations, using the commercial code of Ansys Fluent 2021 R1. To improve computational convergence, the pressure-based coupled algorithm was adopted, and second-order upwind scheme was applied to the spatial discretization, except the transport equation of turbulent scalar. The first-order implicit method was used for the time discretization of transient state.

5. Results

The calculational model was validated by comparison with the thrust and combustion performance obtained from experimental results. Characteristic velocity defined by Eq. (6) is a measure for the engine's combustion performance. Thrust is obtained by Eq. (7) consisting of contributions from momentum and pressure differences. In the calculation of thrust, the exhaust velocity and the pressure at the exit were obtained by mass-weighted average and area-weighted one over the nozzle exit, respectively.

$$C^* = \frac{P_c \cdot A_t}{\dot{m}_t} \tag{6}$$

$$F = \dot{m}_t \cdot v_e + (P_e - P_a)A_e \tag{7}$$

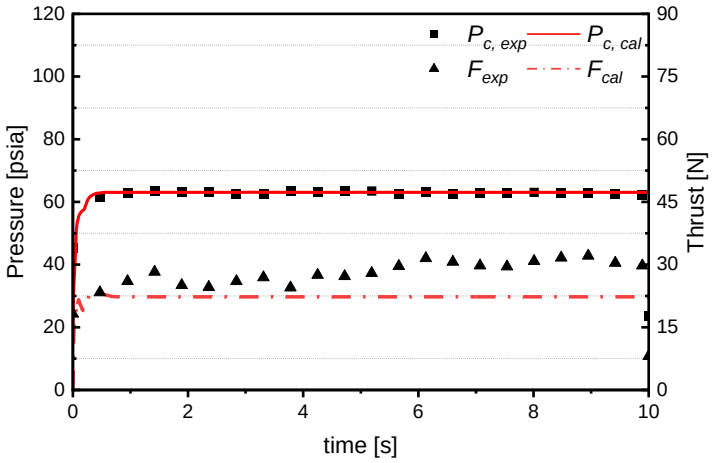

Fig. 3. Comparison of chamber pressure and thrust over time between simulation and experimental results for GE1 case.

Table 3. Comparison of the performance values for GE1.

(I): EIG +3.01 ~ 5.00 s				**(II): ECO -3.51 ~ -0.50 s**			
Case	P_c [psia]	F [N]	C^* [m/s]	Case	P_c [psia]	F [N]	C^* [m/s]
Experiment	63.0	29.1	1647.3	Experiment	62.8	30.5	1648.3
Calculation	63.1	22.3	1649.0	Calculation	63.1	22.3	1649.1

5.1. GE1 case

Fig. 3 shows the variations of thrust and chamber pressure over time for the GE1 case. Numerical comparison of the simulation to the experimental results is summarized in Table 3. An abrupt increase in thrust and pressure that occurs typically at the later stage over the combustion duration didn't happen for the GE1 case. The calculated pressure is in good agreement with the experimental one in Fig. 3. However, a noticeable difference of the thrust values between the calculation and experiment is found. In fact, that was caused by a partial erosion of the nozzle and subsequent expansion of throat area during experiment, resulting in an excessive thrust than expected.

5.2. GE6 case

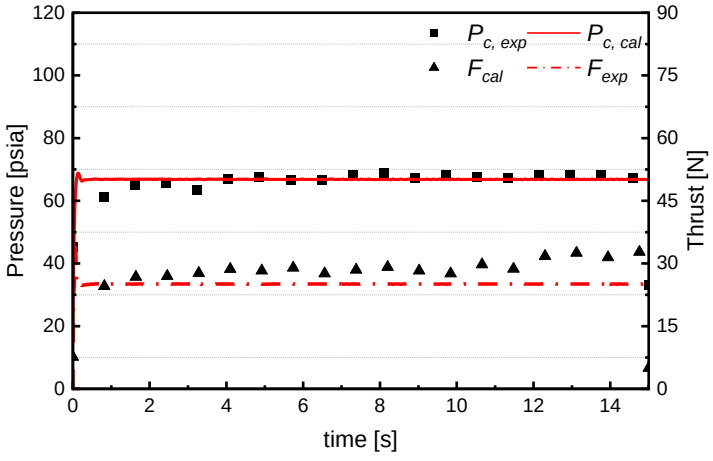

Fig. 4. Comparison of chamber pressure and thrust over time between simulation and experimental results for GE6 case.

Table 4. Comparison of the performance values for GE6.

(I): EIG +3.01 ~ 5.00 s				(II): ECO -3.51 ~ -0.50 s			
Case	P_c [psia]	F [N]	C^* [m/s]	Case	P_c [psia]	F [N]	C^* [m/s]
Experiment	66.5	28.3	1373.7	Experiment	68.2	29.3	1404.2
Calculation	66.9	25.1	1379.8	Calculation	66.8	25.1	1377.7

The results of the GE6 case are summarized in Fig. 4 and Table 4. GE6 case experiment exhibited a slight increase in both pressure and thrust over time. This gradual performance enhancement could not be observed during the firing test of GE1. Meanwhile, the analysis results indicated no escalation of both performance parameters over time and the values remained steady from the beginning phase. This leads to a gradual deviation from the test values towards the end of the combustion.

5.3. GE11 case

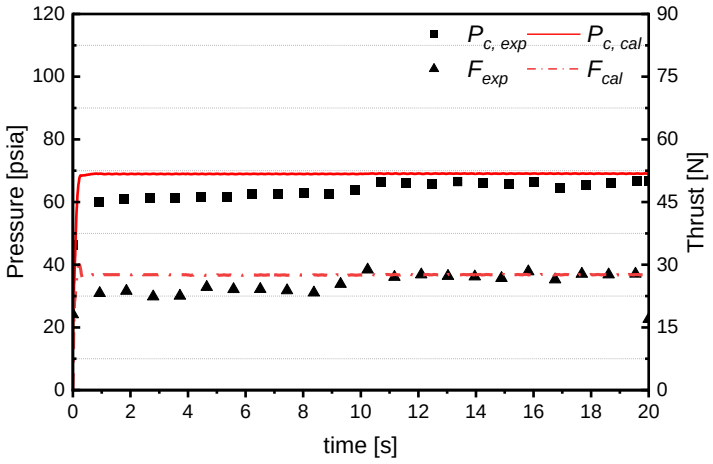

Fig. 5. Comparison of chamber pressure and thrust over time between simulation and experimental results for GE11 case.

Table 5. comparison of the performance values for GE11.

(I): EIG +3.01 ~ 5.00 s				(II): ECO -3.51 ~ -0.50 s			
Case	P_c [psia]	F [N]	C^* [m/s]	Case	P_c [psia]	F [N]	C^* [m/s]
Experiment	61.4	24.0	1045.7	Experiment	66.0	27.5	1115.0
Calculation	68.6	27.3	1167.7	Calculation	69.1	27.3	1176.2

Lastly, the calculation results of the GE11 case are compared to the experimental values, as shown in Fig. 5 and Table 5. GE11 case has the most significant variation in pressure and thrust over time, which can be observed through the sudden augmentation around 10 seconds from ignition in the graph. Though the simulation, however both parameters reach steady as quickly as in the previous cases, and the abnormal performance change found in the test is not observed. This deviation from test results means that the combustion model, in which the mixing and reaction processes are determined by the mixture fraction, is unable to capture the unsteady physics. Therefore, a variation of the combustion model and additional calculation effort are needed for clarifying the unusual phenomena.

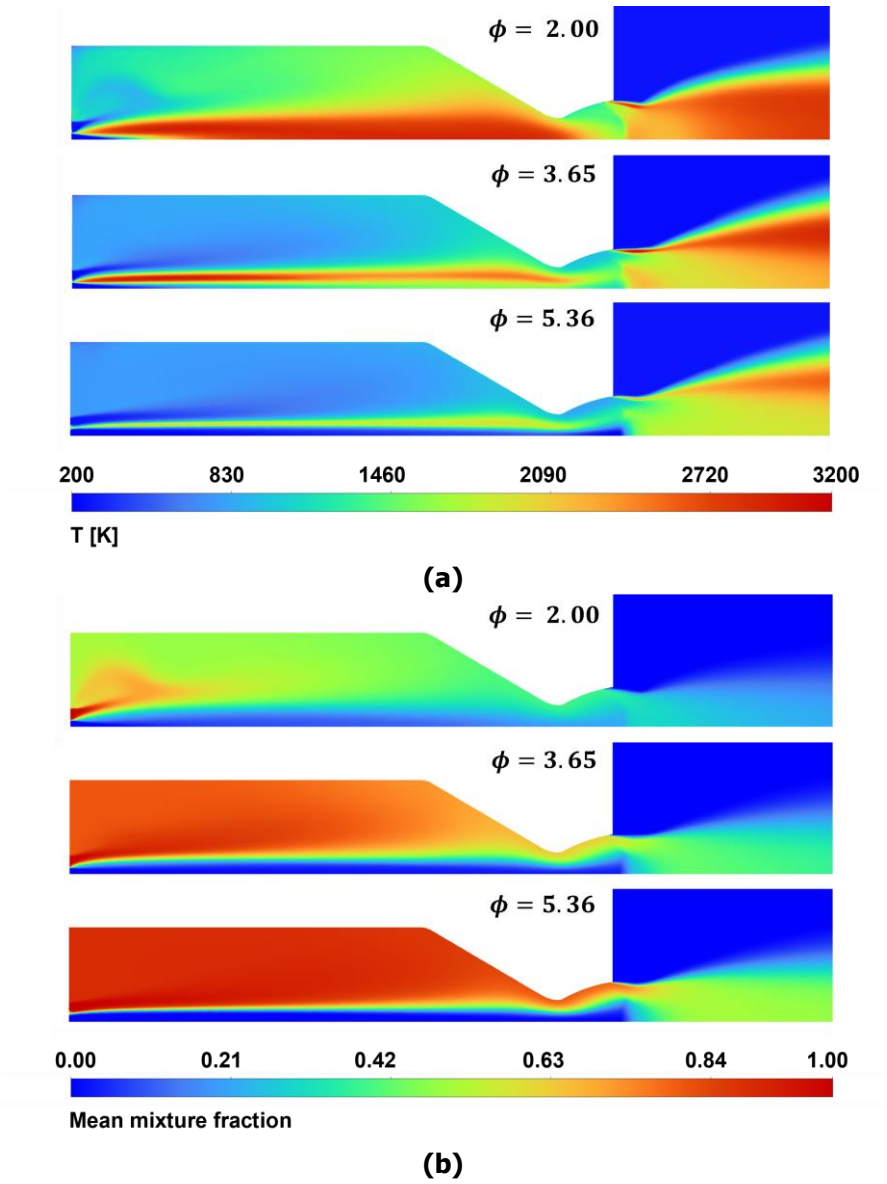

Fig. 6. Distribution of (a) temperature and (b) mean mixture fraction.

5.4. Flame Structure

Fig. 6 presents the distribution of the temperature and mixture fraction varying with equivalence ratio. It is clearly observed that the flame intensity weakens along with a reduction of flame region in the combustion chamber, as the mass flow rate of methane increases, leading to farther deviation from the stoichiometry. GE1 case with an equivalence ratio of 2 has a wide flame structure extended up to the throat of nozzle. The results also show that as the equivalence ratio increases, the fuel-rich region inside the chamber is enlarged and high temperatures form around the stoichiometric mixture fraction of 0.2.

6. Conclusion

A numerical analysis on the combustion behavior of the GCH_4-GOx thrust chamber was conducted as a pathway to establishing a calculation method for predicting the combustion performance of a liquid rocket engine. This study has focused on simulating the unsteady physics which shows a stepwise increase of thrust performance in the later part of the combustion under the very fuel-rich conditions. A non-adiabatic flamelet model with 21 species and 84 reactions was selected to simulate the flame structure. All cases were analysed in a transient state to observe the variations in thrust performance over time.

As a result, the calculated thrust and chamber pressure showed acceptable accuracy overall, but an abnormal performance change observed from the practical firing test was not captured in the numerical calculation. It was inferred that this deviation from test results had been caused by a limitation of the combustion model which could not predict the unsteady physics more realistically. Therefore, additional calculation efforts are needed to clarify the unusual phenomena.

Acknowledgements

This work was supported by the National Research Foundation (NRF) of Korea funded by the Ministry of Science and ICT under Grant (NRF-2022M1A3C2085070) and the Technology Innovation Program (20026368) funded by the Ministry of Trade, Industry & Energy (MOTIE, Korea).

References

1. Cheng, G. C., and Farmer, R. C.: CFD SPRAY COMBUSTION MODEL FOR LIQUID ROCKET ENGINE INJECTOR ANALYSES. 40th AIAA Aerospace Sciences Meeting & Exhibit. (2002). https://doi.org/10.2514/6.2002-785
2. Liang, P. Y., Fisher, S. and Chang, Y. M.: Comprehensive modeling of a liquid rocket combustion chamber. Journal of Propulsion and Power. (1986). https://doi.org/10.2514/3.22851
3. Urbano, A., Selle, L., Staffelbach, G., Cuenot, B., Schmitt, T., Ducruix, S., and Candel, S.: Exploration of combustion instability triggering using Large Eddy Simulation of a multiple injector liquid rocket engine, Journal of Combustion and Flame. (2016). https://doi.org/10.1016/j.combustflame.2016.03.020
4. Kang, Y. H., Ahn, H. J., Bae C. H. and Kim, J. S.: Combustion Characteristics of the Gaseous-methane & Gaseous-oxygen Reactants under Highly Fuel-rich Conditions. Journal of the Korean Society of Propulsion Engineers (2021). https://doi.org/10.6108/KSPE.2021.25.6.045
5. Shih, T.H., Liou, W. W., Shabbir, A., Yang, Z., and Zhu, J.: A new k-ϵ eddy viscosity model for high Reynolds number turbulent flows. Computers & Fluids. 24(3). 227-238. (1995)
6. Sakar, S., Erlebacher, G., Hussaini, M. Y., and Kreiss, H. O.: The Analysis and Modelling of Dilatational Terms in Compressible Turbulence. Journal of Fluid Mechanics. (1991). https://doi.org/10.1017/S0022112091000204
7. Gerald J.M. and Helldorff, H. V. A.: Compressible Turbulence Model for High-speed Flows. Florida Institute of Technology. IOP Publishing ResearchGate. https://www.Researchgate.net/publication/344933934_A_Compressible_Turbulence_Model_for_High_Speed_Flows. (2020). Accessed 20 March 2024
8. Peters, N.: Laminar diffusion flamelet models in non-premixed turbulent combustion. Progress in Energy and Combustion Science. 10(3). 319-339. (1984)
9. Breda, P., Pfitzner, M., Perakis, N., and Haidn, O.J.: Generation of non-adiabatic flamelet manifolds: comparison of two approaches applied on a single-element GCH_4/GO_2 combustion chamber. 8th European Conference for Aeronautics and Aerospace Sciences (EUCASS). (2019). https://doi.org/10.13009/EUCASS2019-121
10. Pitsch, H., and Peters, N.: A Consistent Flamelet Formulation for Non-Premixed Combustion Considering Differential Diffusion Effects. Combustion And Flame. 114. 26-40. (1998)
11. Chang, W. C. and Chen, J. Y.: Reduced Reaction Sets based on GRI-Mech 1.2. http://combustion.berkeley.edu/drm/drm19.dat. Accessed 20 March 2024
12. McBride, B. J. and Gordon, S.: Computer Program for Calculation of Complex Chemical Equilibrium Compositions and Applications, NASA Reference Publication 1311. (1996)